JOURNAL OF COMPUTATIONAL PHYSICS 66, 21–35 (1986)

High-Frequency Numerical-Analytic Approximations for the Separable Acoustic Wave Equation

J. R. BRANNAN AND G. P. FORNEY

Department of Mathematical Sciences, Clemson University, Clemson, South Carolina 29631

AND

R. F. HENRICK*

The Johns Hopkins University, Applied Physics Laboratory, Johns Hopkins Road, Laurel, Maryland 20707

Received October 16, 1984; revised July 31, 1985

An algorithm which employs a combination of asymptotic and numerical methods to solve a Sturm–Liouville problem arising from a separable acoustic wave equation is presented. Error criteria for switching between methods are derived. Implementation requires a decomposition of the index of refraction profile into separable subprofiles. Computing times and accuracies are compared with conventional methods. © 1986 Academic Press, Inc.

1. INTRODUCTION

Solving th Helmholtz equation by strictly using only numerical methods becomes increasingly difficult and time-consuming as the frequency of the wave increases. In representing broadband and pulsed wave propagation by frequency integrals the problem is compounded since the Helmholtz equation must be solved at a large enough number of frequencies to accurately represent the time-dependent pressure field.

If the Helmholtz equation is separable and the frequencies of interest are not too low, it is possible to take advantage of high-frequency asymptotics to alleviate some of the computational burden. The primary difficulty encountered in the implementation of the asymptotics is that of obtaining approximations which are uniformly valid over the domain of interest. For simple sound speed profiles involving only one or two turning points the method of matched asymptotic expansions can provide uniformly valid analytic approximations [1]. However, if there are more than two turning points present, as occurs in sound speed profiles with multiple

* Present address: BBN Laboratories, 1300 North 17th Street, Arlington, Virginia 22209.

0021-9991/86 $3.00

channels, strict use of asymptotics becomes prohibitively complicated. Furthermore, sound speed profiles or indices of refraction are often represented by linear interpolation between data points. Since a derivative of the profile at a turning point is required for the turning point analysis, the issue is further complicated when turning points are near sound speed data points.

In this paper we describe a solution scheme which combines both numerical and asymptotic methods to produce uniformly valid approximations. The basic strategy is simple: use asymptotic expressions whenever they are valid approximations. This results in a reasonably accurate code with run times in excess of one order of magnitude faster than conventional codes and can in addition handle extremely high frequencies. These features make it particularly attractive for broadband and pulsed propagation problems. This work is a report on the general theory which provides a significant extension of the approach used in Ref.[2] to complex sound speed profiles and varying medium densities.

In Section 2 we discuss the problem to be solved. In Section 3 are presented error criteria for deciding where to switch from asymptotics to numerics and vice versa. In Section 4 we discuss the decomposition of index of refraction (IOR) profiles into subprofiles amenable to combined asymptotic and numerical treatment. In Section 5 examples are presented and limitations of the model are discussed.

2. Statement of the Problem

The acoustic pressure produced by a point source with arbitrary time t dependence has the Fourier representation

$$p(r, z, t) = \frac{1}{2\pi} \int_{-\infty}^{\infty} P(r, z, \omega)\, F(\omega)\, e^{-i\omega t} d\omega \tag{1}$$

where ω is angular frequency, $F(\omega)$ is the Fourier transform of the source waveform, and P is the frequency response of the channel. For a vertically stratified channel of depth h with rigid bottom and pressure release surface, P is obtained from the separable Helmholtz equation in cylindrical coordinates

$$\frac{\partial^2 P}{\partial r^2} + \frac{1}{r}\frac{\partial_p}{\partial r} + \frac{\partial^2 P}{\partial z^2} - \frac{1}{\rho}\frac{d\rho}{dz}\frac{\partial P}{\partial z} + k^2(z)\, P = -\delta(r)\, \delta(z - z_0)/2\pi r \tag{2}$$

along with boundary conditions

$$\frac{\partial P}{\partial z}(r, -h) = P(r, 0) = 0. \tag{3}$$

In Eq. (2), r = receiver range, z = receiver depth, z_0 = source depth, $\rho(z)$ = medium density, $c(z)$ = medium sound speed, $n(z) = c(0)/c(z)$ = index of refraction, and

$k = \omega/c(0) =$ wave number. The solution to Eqs. (2) and (3) in the normal mode representation [2] is

$$P(r, z, \omega) = \frac{i}{4} \frac{1}{\rho(z_0)} \sum_{m=1}^{\infty} \phi_m(z_0)\, \phi_m(z)\, H_0^{(1)}(k a_m r) \Big/ \int_{-h}^{0} \rho^{-1}(s)\, \phi^2{}_m(s)\, ds \qquad (4)$$

where $H_0^{(1)}$ is the Hankel function of order zero of the first kind and the eigenvalues a_m and eigenfunctions ϕ_m are solutions of the Sturm–Liouville problem

$$(\rho^{-1}(z)\, \phi')' + k^2 \rho^{-1}(z)(n^2(z) - a^2)\, \phi = 0 \qquad (5)$$

with boundary conditions

$$\phi(0) = \phi(-h) = 0. \qquad (6)$$

Numerical evaluation of Eq. (1) requires replacing the infinite limits with finite limits corresponding to the bandwidth of the signal, approximating the resulting integral with a sum and evaluating the sum for a discrete set of values of α. Accuracy requirements generally require values of P, and hence solutions to Eqs. (5) and (6), at a large number of frequency grid points. Common numerical methods for solving Eqs. (5) and (6) are shooting methods [3], local coefficient approximation methods [4], finite elements [5], and finite difference methods with refinements [6]. In all these methods grid resolution must increase with frequency in order to achieve satisfactory accuracy. In this paper we instead use high-frequency asymptotics, the WKB method, to represent solutions of Eqs. (5) and (6) wherever possible.

The normal mode representation in (4) is possible since the variables for the problem (2)–(3) separate due to the fact that the environment is range-independent. For range-dependent environments, i.e., where the depth or sound speed varies with range, our method will not work unless, for example, an adiabatic approximation for slowly changing range dependence is used [7] or the range interval is divided into segments with vertical boundaries of distributed sources where the solution within each segment is computed in a range-independent manner [8]. A natural approach to solving the Helmholtz equation in range-dependent environments is by finite element or finite difference methods. These approaches have several merits but high-frequency and multiple-frequency runs still require considerable storage and time. In order to limit the area of computation by these methods artificial absorbing boundary conditions have been developed which minimize undesirable, extraneous wall reflections [9–11]. The radiation condition at infinity is accounted for in (4) by the proper selection of the eigenfunction expansion. We finally remark that there is usually a very limited amount of data available to characterize well range-dependent environments. For a comprehensive survey of range-independent and range-dependent numerical models of underwater acoustic propagation, see [2].

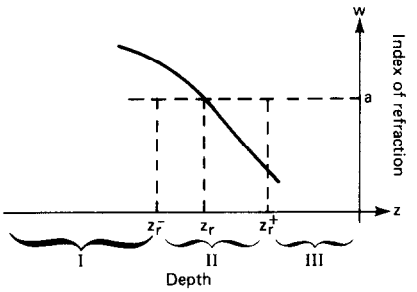

FIG. 1. Illustration of decomposition of index of refraction profile near a mode turning point.

3. Determining Asymptotic and Numerical Regions

Consider the graph in Fig. 1 of a portion of the function $w = n(z)$ and the constant function $w = a$. In region I where $q = n^2 - a^2 > 0$, the physical optics [13] approximation to the general solution of Eq. (5) is

$$\phi_{\mathrm{I,WKB}}(z) \sim A_1 \phi^{(1)}_{\mathrm{I,WKB}}(z) + A_2 \phi^{(2)}_{\mathrm{I,WKB}}(z) \tag{7}$$
$$= \rho^{1/2} q^{-1/4} \left[A_1 \exp\left(-ik \int_z^{z_r} q^{1/2}(s)\, ds \right) + A_2 \exp\left(ik \int_z^{z_r} q^{1/2}(s)\, ds \right) \right], \quad q > 0$$

and in region III where $r = a^2 - n^2 > 0$, the physical optics approximation to the general solution of Eq. (5) is

$$\phi_{\mathrm{III,WKB}}(z) \sim C_1 \phi^{(1)}_{\mathrm{III,WKB}}(z) + C_2 \phi^{(2)}_{\mathrm{III,WKB}}(z) \tag{8}$$
$$= \rho^{1/2} r^{-1/4} \left[C_1 \exp\left(-k \int_{z_T}^{z} r^{1/2}(s)\, ds \right) + C_2 \exp\left(k \int_{z_T}^{z} r^{1/2}(s)\, ds \right) \right], \quad r > 0.$$

As z approaches the right turning point $z = z_r$, the error between these WKB approximations and the exact solution approaches ∞ since $q(z), r(z) \to 0$ as $z \to z_r$. Thus, we need to determine the size of region II $= (z_r^-, z_r^+)$ outside of which the difference between the WKB approximations and the exact solutions of Eq. (5) remains less than some prescribed error bound. In region I we write Eq. (5) in the form

$$(\rho^{-1}\phi')' + \rho^{-1}(k^2 q + h_1)\,\phi = \rho^{-1} h_1 \phi, \qquad q > 0 \tag{9}$$

where

$$h_1 = h_1(z) = \frac{1}{4}\frac{q''}{q} - \frac{5}{16}\left(\frac{q'}{q}\right)^2 - \frac{1}{2}\frac{\rho''}{\rho} + \frac{3}{4}\left(\frac{\rho'}{\rho}\right)^2 \tag{10}$$

and in region III we write Eq. (5) in the form

$$(\rho^{-1}\phi')' + \rho^{-1}(k^2 q + h_3)\,\phi = \rho^{-1} h_3 \phi, \qquad q < 0 \tag{11}$$

where

$$h_3 = h_3(z) = \frac{1}{4}\frac{r''}{r} - \frac{5}{16}\left(\frac{r'}{r}\right)^2 - \frac{1}{2}\frac{\rho''}{\rho} + \frac{3}{4}\left(\frac{\rho'}{\rho}\right)^2. \tag{12}$$

Since $\phi_{\mathrm{I,WKB}}$ satisfies Eq. (9) exactly when the right-hand side is set to 0, the variation of parameters formula in differential equations allows us to write Eq. (9) in the integral form

$$\phi^{(j)}(z) = \phi^{(j)}_{\mathrm{I,WKB}} + k^{-1}\rho^{1/2}(z)\, q^{-1/4}(z) \int_z^{z_r^-} \rho^{-1/2}(t)\, q^{-1/4}(t)$$

$$\times \sin\left[k \int_t^z q^{1/2}(s)\, ds\right] h_1(t)\, \phi^{(j)}(t)\, dt, \tag{13}$$

$j = 1, 2$, where we have denoted the exact solution by $\phi^{(j)}(z)$. Similarly, Eq. (11) may be written as

$$\phi^{(j)}(z) = \phi^{(j)}_{\mathrm{III,WKB}} + k^{-1}\rho^{1/2}(z)\, r^{-1/4}(z) \int_{z_r^+}^z \rho^{-1/2}(t)\, r^{-1/4}(t)$$

$$\times \sinh\left[k \int_t^z r^{1/2}(s)\, ds\right] h_3(t)\, \phi^{(j)}(t)\, dt, \tag{14}$$

$j = 1, 2$. Using the method of successive approximations [14] on Eqs. (13) and (14) we obtain the error bounds

$$|\phi^{(j)}(z) - \phi^{(j)}_{\mathrm{I,WKB}}(z)| \leqslant \rho^{1/2}(z)\, q^{-1/4}(z)[e^{U_1(z_t^- - z)/k} - 1], \qquad z < z_r^- \tag{15}$$

where

$$U_1 = \max_{t \in [z, z_r^-]} |q^{-1/2}(t)\, h_1(t)| \tag{16}$$

and

$$|\phi^{(j)}(z) - \phi^{(j)}_{\mathrm{III,WKB}}(z)| \leqslant \rho^{1/2}(z)\, r^{-1/4}(z)\, e^{(-1)/k} \int_{z_T}^{z_T^+} r^{1/2}(s)\, ds$$

$$\cdot [e^{U_3 F(z)(z - z_T^+)/k} - 1], \qquad z > z_r^+ \tag{17}$$

where

$$U_3 = \max_{t \in [z_r^+, z]} |q^{-1/2}(t)\, h_3(t)| \tag{18}$$

and

$$F(z) = \sinh\left[k \int_{z_r^+}^{z} r^{1/2}(d)\, ds\right]. \tag{19}$$

One of the mysteries about high-frequency asymptotics is why they work so well even when the frequency is not high. From the terms in U_1, it is clear that if the product of density and sound speed gradients and curvatures within the channel width are small relative to the frequency and z_r^- is not too near z_r, then the bound in Eq. (15) will be small. In water ρ is essentially constant and sound speed rarely varies more than a few percent over the water column. In sediment layers sound speed gradients are larger and the errors incurred are therefore larger than in the water column. Fortunately, attenuation effects in sediment layers are higher also so these errors are not serious. If $z_r^+ - z_r$ is sufficiently large and z is not significantly larger than z_r^+ then the absolute error between $\phi^{(1)}(z)$ and $\phi_{\mathrm{III,WKB}}(z)$ will be small but not the relative error. The situation is reversed for $\phi^{(2)}(z)$ and $\phi_{\mathrm{III,WKB}}(z)$.

To find the width of region II, assume that the maximum in Eq. (16) occurs when t is nearest the turning point, i.e., at $t = z_r^-$. From (15) then we obtain

$$|\phi^{(j)}(z) - \phi^{(j)}_{\mathrm{I,WKB}}(z)| \leqslant H[q'(z_T^-)]^2/k[q(z_T^-)]^{11/4} + \cdots \tag{20}$$

where H is a measure of channel width. Requiring the right-hand side of (17) to be less than some prescribed error bound ε_1 yields z_r^-. For z_r^+ we use the simpler criterion

$$k \int_{z_r}^{z_r^+} r^{1/2}(s)\, ds \geqslant \varepsilon_2^{-1} \tag{21}$$

where ε_2 is a prescribed error bound.

In region II Eq. (5) is very easy to solve numerically since $|k^2\rho^{-1}(n^2 - a^2)| \ll 1$. The following matching conditions are used at the transition point z_r^-

$$\phi_{\mathrm{I,WKB}}(z_r^-) = \phi_{\mathrm{II}}(z_r^-) \tag{22}$$

$$\rho^{-1}(z_r^-)\, \phi'_{\mathrm{I,WKB}}(z_r^-) = \rho^{-1}(z_r^-)\, \phi'_{\mathrm{II}}(z_r^-) \tag{23}$$

and similarly at $z = z_r^+$. We remark that three terms are carried in the WKB expressions for the purposes of computing derivatives in order to keep the errors proportional to k^{-1}.

4. Profile Decomposition and Classification

In order to implement the WKB solutions for the total IOR profile we decompose the profile into subprofiles which possess one or two turning points with the possible presence of at most two discontinuities in the interiors of the subprofiles.

Associated with each subprofile is an ordered pair of integers (i_{j1}, i_{j2}) were j refers to the jth profile. The first integer (i_{j1}) refers to the type of intersection made by the separation constant, a, and the profile $n(z)$. The second integer (i_{j2}) refers to the number of profile discontinuities between the intersection points. Also associated with each subprofile is a pair of depths (z_{j1}, z_{j2}) which bracket the depth data points defining $n(z)$ for that subprofile. In addition it is also necessary to record the values of transition levels of the separation constant, a, which form the boundaries between subprofiles in the vertical direction. The upper limit is denoted by a_{jT} and the lower limit is denoted by a_{jB}. Each subprofile has associated with it an eigenvalue condition determined by the types of intersection that the separation constant, a, makes with $n(z)$. The possible intersection types are surface (S), turning point (TP), discontinuity (D), and bottom (B). Since the vertical boundaries are determined by a change in the types of intersection, the eigenvalue condition is not valid throughout the interval $[a_{jB}, a_{jT}]$ but only on a subinterval $[\tilde{a}_{jB}, \tilde{a}_{jT}] \subset [a_{jB}, a_{jT}]$ where $a_{jB} < \tilde{a}_{jB}$ and $\tilde{a}_{jT} < a_{jT}$. $\tilde{a}_{jB}$ and $\tilde{a}_{jT}$ are determined by application of the error criteria discussed in Section 3. The vertical intervals $(a_{jB}, \tilde{a}_{jB})$ and $(\tilde{a}_{jT}, a_{jT})$ are called criterial regions and special eigenvalue conditions are associated with each critical region. The critical regions arise because a turning point may get close to a surface or bottom boundary, a discontinuity, or a local sound speed maximum (tunnel or top of a barrier). If $\tilde{a}_{jB} > \tilde{a}_{jT}$, then the entire subprofile becomes a critical region.

Figure 2 illustrates a decomposition for a sample IOR profile. Subprofiles 1 and 3 are TP, S types, subprofile 2 is a TP, TP type, subprofile 4 is a D, S type, subprofile 5 is a TP, D, S type, and subprofile 6 is a B, S type. The eigenvalue condition for the noncritical region of subprofile 2 is [7]

$$\sin\left[k\int_{z_{2l}(a)}^{z_{2r}(a)} q^{1/2}(s)\,ds + \frac{\pi}{2}\right] = 0, \qquad a \in [\tilde{\alpha}_{2B}, \tilde{\alpha}_{2T}] \tag{24}$$

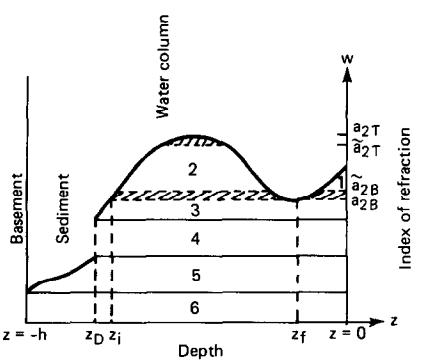

FIG. 2. Illustration of decomposition of index of refraction profile into subprofiles.

where $z_{2l}(a)$ and $z_{2r}(a)$ are the abscissas of the left and right turning points, respectively. If a_m is an eigenvalue the corresponding asymptotic representation of the eigenfunction and squared norm are

$$\phi_m(z) \sim \sin\left[k\int_{z_{2l}(a_m)}^{z}\sqrt{n^2(s)-a_m^2}\,ds+\frac{\pi}{4}\right] \tag{25}$$

and

$$\int_{-h}^{0}\rho^{-1}(s)\,\phi_m^2(s)\,ds \sim 1/2\int_{z_{2l}(a_m)}^{z_{2r}(a_m)}[n^2(s)-a_m^2]^{-1/2}\,ds \tag{26}$$

respectively. The eigenvalue condition for the noncritical region of subprofile 5 is more complicated. The general WKB solution valid for $z<z_D$ and $q(z)>0$ which is the continuation of the WKB solution that exponentially decays into the bottom (and therefore approximately satisfies the bottom boundary condition $\phi'(-h)=0$), is

$$A\phi^{(1)}(z_{5l}(a), z; a) = A\rho^{1/2}(z)\,q^{-1/4}(z)\sin\left[k\int_{z_{5l}(a)}^{z}q^{1/2}(s)\,ds+\frac{\pi}{4}\right], \qquad z_{5l}^{+}(a)<z\leqslant z_D, \tag{27}$$

The general WKB solution valid for $z_D<z<0$ and $q(z)>0$ is

$$B\phi^{(1)}(z_D, z; a)+C\phi^{(2)}(z_D, z; a) = \rho^{1/2}(z)\,q^{-1/4}(z)\left\{B\sin\left[k\int_{z_D}^{z}q^{1/2}(s)\,ds+\frac{\pi}{4}\right]\right. \left.+\,C\cos\left[k\int_{z_D}^{z}q^{1/2}(s)\,ds+\frac{\pi}{4}\right]\right\}, \qquad z_D\leqslant z\leqslant 0. \tag{28}$$

Requiring continuity of ϕ and $\rho^{-1}\phi'$ at $z=z_D$ and satisfying the surface boundary conditions leads to the problem

$$A_{3\times 3}(a)\,X_{3\times 1}=0 \tag{29}$$

where

$$A_{3\times 3}(a)= \begin{bmatrix} \phi^{(1)}(z_{5l}(a), z_D^{-}; a) & -\phi^{(1)}(z_D, z_D^{+}; a) & -\phi^{(2)}(z_D, z_D^{+}; a) \\ \rho^{-1}(z_D^{-})\phi_z^{(1)}(z_{5l}(a), z_D^{-}; a) & \rho^{-1}(z_D^{+})\phi_z^{(1)}(z_{5l}(a), z_D^{+}; a) & \rho^{-1}(z_D^{+})\phi_z^{(2)}(z_{5l}(a), z_D^{+}; a) \\ 0 & \phi^{(1)}(z_{5l}(a), 0; a) & \phi^{(2)}(z_{5l}(a); 0; a) \end{bmatrix} \tag{30}$$

and

$$X_{3\times 1} = \begin{pmatrix} A \\ B \\ C \end{pmatrix}. \tag{31}$$

The requirement for nontrivial calculations yields the eigenvalue condition

$$\det A_{3\times 3}(a) = 0, \qquad a \in [\tilde{a}_{5B}, \tilde{a}_{5T}]. \tag{32}$$

Having found the eigenvalues $a_m \in [a_{5B}, a_{5T}]$, the asymptotic expression for the mode normalization is

$$\int_{-h}^{0} \rho^{-1}(s)\, \phi_m^2(s)\, ds \sim \frac{1}{2} A_m^2 \int_{z_l(a_m)}^{z_D} [n^2(s) - a_m^2]^{-1/2} ds + \frac{1}{2} [B_m^2 + C_m^2] \int_{z_D}^{z} [n^2(s) - a_m^2]^{-1/2} ds. \tag{33}$$

Asymptotic formulas may also be derived for attenuation factors which are devised by a perturbative method. The other noncritical regions are handled similarly.

As an example of how a critical region is handled, consider $[a_{5B}, \tilde{a}_{5B}]$. In this case one numerically constructs a solution which satisfies the bottom boundary condition at $z = -h$ to the depth $z = z_l^+(a)$ where the WKB solution is valid. Then continuity of ϕ and $\rho^{-1}\phi'$ are applied at $z = z_l^+(a)$, $z = z_D$ and satisfying the surface boundary condition leads to a 5×5 determinantal eigenvalue condition.

The bottom critical region of subprofiles 2 and 1 is combined with the top critical region of subprofile 3 into a tunnel region. The solution to Eq. (5) in the neighborhood of the sound speed maximum is then constructed numerically. Satisfying boundary conditions and continuity requirements with adjacent WKB solutions leads to another eigenvalue condition.

5. Accuracy Comparisons

To illustrate both the accuracy and limitations of the uniform asymptotic approach, we consider calculation of transmission loss (ten times the logarithm of intensity at a given range relative to intensity at one meter) in a deep ocean environment. For accuracy comparisons, a numerical code developed by the Naval Research Laboratories [15], which employs strict numerical techniques, is utilized. The environment chosen is illustrated in Fig. 3. The sound speed profile illustrates minimum (index of refraction maximum) at the surface and at a depth of 800 m. A sound speed maximum (index of refraction minima) occurs at 100 m. The sediment velocity profile shows a discontinuity at the water/sediment interface and a strong increase in sound speed. In addition, a strong density discontinuity also exists. The

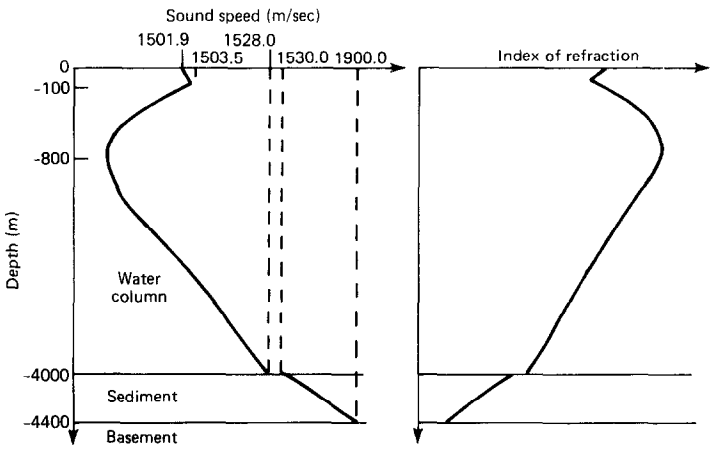

FIG. 3. Sound speed and index of refraction profile used in comparison. Sediment attenuation = 0.05 dB/m/kHz.

sound speed minimum at the surface forms an acoustic duct. Geometrical optics (ray theory) would predict that a source in the duct (above 100 m depth) would excite waves trapped in the duct. However, LaBianca [16] has shown that at frequencies below about 300 Hz, diffractive leakage will make the duct acoustically insignificant. For our comparison, we use a source and receiver depth of 50 m, and a frequency of 100 Hz, selections which will illustrate the importance of diffraction.

From Eq. (4), the pressure field P is computed from a modal sum whose only range dependence arises through the oscillatory complex exponential and the attenuation damping. Thus, the range behavior is determined by the eigenvalues a_n and attenuation α_n. To compare these quantities, two more physically meaningful quantities are defined, the phase velocity V_n and dB loss in 100 km D_n:

$$V_n = c_0/a_n \tag{34}$$

and

$$D_n = 8.6 \times 10^5 \alpha_n. \tag{35}$$

The phase velocity yields physical insight into the vertical extent of the energy carried by the mode; the mode is oscillatory for sound speeds less then the phase velocity and exponentially damped when sound speed is greater than the phase velocity. The quantity D_n defines how quickly a given mode is attenuated by water or sediment absorption. Table I presents a comparison of phase velocity and attenuation for three separate groups of modes: one group with V_n much less then the bottom sound speed of 1527.5 m/sec (water column refracted), one group with V_n near the sound speed at the top of the sediment (weak interaction with

TABLE I

Phase Velocity and Attenuation Comparisons between NRL Numeric and WKB Asymptotic-Numeric Codes

	Phase velocities (m/sec)		Attenuation in 100 km (dB)	
Mode No.	NRL	WKB	NRL	WKB
28	1502.188	1502.194	0.120	0.120
29	1502.590	1502.596	0.120	0.120
30	1502.984	1502.991	0.120	0.120
31	1503.372	1502.378	0.120	0.120
⋮				
94	1529.257	1529.260	1.47	1.40
95	1529.712	1529.715	1.65	1.60
96	1530.177	1530.184	1.76	1.76
97	1530.653	1530.659	1.86	1.85
⋮				
187	1603.275	1603.458	16.4	16.3
188	1604.417	1604.611	14.5	14.5
189	1605.572	1605.776	13.4	13.4
190	1606.737	1606.952	12.7	12.7

sediment), and a third group with a sound speed much higher than that of the top of the sediment (strong penetration into the sediment). The attenuation values reflect the interaction with the sediment, showing an increase from less than 1 dB attenuation from water absorption for the first group and over 10 dB for the sediment penetration modes. Attenuation values computed with the WKB code agree to a fraction of a dB with those computed by the NRL code.

The eigenvalue comparison illustrates that the uniform WKB eigenvalues agree with the NRL numerically generated values for six to seven decimal places for the first two groups. A significantly larger error is noted for the modes that penetrate depth into the bottom. This error results from the presence of large vertical sound speed gradients in the sediment. From Eq. (10), (12), and (15)–(19), the error increases as the index of refraction (equivalently sound speed) gradient grows. In the sediment, these gradients are two orders of magnitude larger than those encountered in the water column. However, Table I indicates that attenuation values are accurate, and a comparison of mode amplitudes (not presented here) also indicates similar accuracy. Further, it is not the magnitude of the eigenvalues that determines the modal interference pattern in Eq. (9), but rather the relative separation between eigenvalues. Tindle and Guthrie [17] have shown that the range at which a bundle of energy associated with a mode completes one cycle through the ocean and sediment is inversely proportional to the separation between phase velocities. This is the first range at which two adjacent modes constructively interfere in the sum of Eq. (4). For example, the NRL code predicts mode 188 to have a cycle distance of 22.48 km while the WKB code predicts a cycle distance of 22.30 km. Although the

phase velocity errors are large for these modes, the error in the separation between phase velocities is much smaller. Given the agreement between mode amplitudes and attenuations, the net effect of the WKB errors results only in a small range shift. These errors are significantly small (particularly with respect to errors arising from predicting sediment properties in several thousand meters of water) that no practical limitations of applicability of technique result here. Further, these errors diminish as frequency increases.

To illustrate the accuracy of the code, the resuls of the modal sums in Eq. (4) for the numeric (NRL) and joint numeric-asymptotic (WKB) approaches are presented in the form of transmission loss. Figure 4 presents a transmission loss comparison if only modes that do not strongly interact with the bottom are included in the sum of Eq. (4); this is accomplished by terminating the sum when mode phase velocities exceed 1527 m/sec. The large fade-outs between peaks indicate that all acoustic energy leaks out of the surface channel, a diffractive effect not included in a geometrical optics approach. The periodic peaks represent energy that has cycled into the deep ocean and returned to the shallow receiver. Good agreement is noted

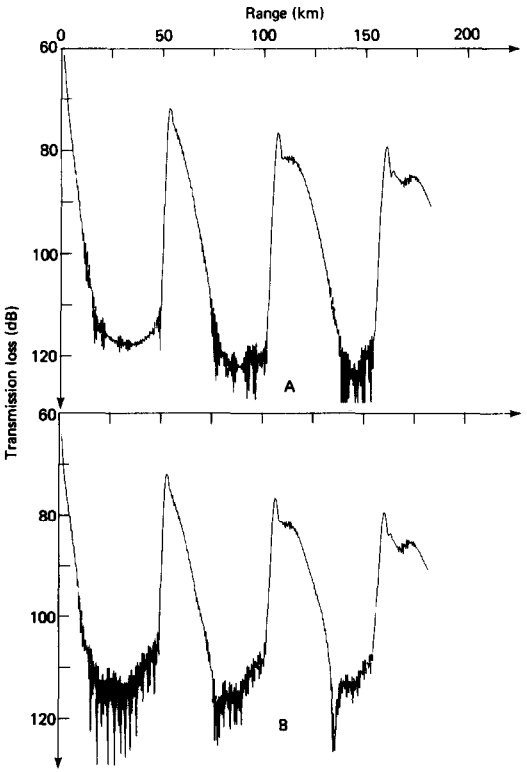

FIG. 4. Comparison of NRL (A) and WKB (B) transmission loss results for propagation of energy not interacting strongly with bottom.

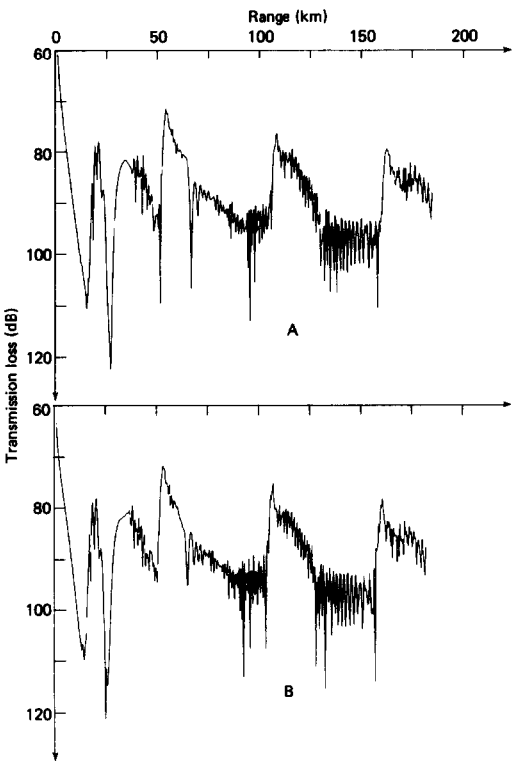

FIG. 5. Comparison of NRL (A) and WKB (B) transmission loss results if bottom interacting energy is included.

between the two codes in both the shapes and levels of the curves. Figure 5 presents a similar comparison, but including modes in Eq. (4) with phase velocities as high as 1700 m/sec. The effect of including the sediment interacting energy is to fill the fade-outs of Fig. 3. Again the agreement in the behavior of the two curves is good. The only discrepancies exist in the magnitudes of the signal fade-outs which arise from two or more bundles of energy arriving at the receiver with opposite phases, resulting in a cancellation. To illustrate the efficiency of the asymptotic approach, the NRL code took 12 minutes of VAX 11/780 CPU time to calculate the quantities needed for the modal sum of Eq. (4). The uniform WKB code took 37 seconds, a savings of over one order of magnitude. These savings become more meaningful if a multiple-frequency pulsed case described in Eq. (1) is considered. If 128 frequencies were required, the NRL code would require roughly 1 day of CPU time versus just over 1 hour for the WKB code. Given the typical real time to CPU time ratio that exists in a multi-user environment, this difference amounts to several runs per day versus one run per week.

6. Summary and Conclusions

A joint analytic-numeric approach is used to solve the separable wave equation in the context of underwater acoustic propagation. The uniform WKB approach is used to obtain approximations to the normal modes of the sound channel. The concept is to use analytical asymptotic approximations where such approximations are valid and numerical techniques in other cases. Error estimates for the analytical formula are derived and utilized to define regions where numerics are necessary. Techniques and expressions to match the analytical solution to the numeric solutions while satisfying the boundary conditions are also presented. The resulting techniques are applicable to the types of sound channels and sediments that arise in underwater acoustic propagation.

A comparison of results obtained from the hybrid approach to those obtained from strict numerical calculation is made. It is shown that accurate approximations are made to the eigenvalues of modes that are trapped in the water column, but that larger errors result for modes that deeply penetrate the sediment. These errors result from the high sound speed gradients in the sediment as illustrated in the derivation of the error estimates. However, the separation between eigenvalues is shown to be less in error and it is argued that this separation is the critical factor in determining the modal interference patterns. A comparison of transmission loss for the two approaches demonstrates that accurate treatment of diffraction in the water column, and the accuracy of predictions of transmission loss for bottom interacting energy. The efficiency of the joint analytic-numeric approach is noted by over an order of magnitude reduction in run time.

In summary, this paper documents both the accuracy and efficiency of using combined analytic and numeric approaches to solve problems of practical interest. Although originally applied to acoustic propagation, such an approach has applications in a wide variety of separable physical problems.

References

1. C. M. Bender and S. A. Orszag, Advanced Mathematical Methods for Scientists and Engineers (McGraw–Hill, New York, 1978).
2. R. F. Henrick, J. R. Brannan, D. B. Warner, and G. P. Forney, *J. Acoust. Soc. Amer.* **74**, 1464 (1983).
3. H. M. Beisner, *IBM J. Res. Dev.* **18**, 53 (1974).
4. D. C. Strickler, *J. Acoust. Soc. Amer.* **57**, 856 (1975).
5. G. Strang and G. J. Fix, An Analysis of the Finite Element Method (Prentice–Hall, Englewood Cliffs, N. J., 1973).
6. M. Porter and E. L. Reiss, *J. Acoust. Soc. Amer.* **76**, 244 (1984).
7. A. Nagl, H. Uberall, A. Haug, and G. Zarur, *J. Acoust. Soc. Amer.* **63**, 739 (1978).
8. W. G. Kanabis, "A Shallow Water Acoustic Model for an Ocean Stratified in Range and Depth," NUSC Technical Report 4887–1, Naval Underwater Systems Center, New London, Conn., 1975, (unpublished).
9. A. Bayliss, M. Gunzburger, and E. Turkel, *SIAM J. Appl. Math.* **42**, 430 (1982).

10. B. ENGQUIST AND A. MADJA, *Math. Comput.* **31**, 629 (1977).
11. G. J. FIX AND S. P. MARIN, *J. Comput. Phys.* **28**, 253 (1978).
12. F. R. DINAPOLI AND R. L. DEAVENPORT, "Numerical Models of Underwater Acoustic Propagation," Topics in Current Physics 8: Ocean Acoustics, edited by J. A. DeSanto (Springer–Verlag, New York, 1979).
13. D. S. AHLUWALIA AND J. B. KELLER, "Exact and Asymptotic Representations of the Sound Field in a Stratified Ocean," Lecture Notes in Physics Vol. 70: Wave Propagation in Underwater Acoustics, edited by J. B. Keller and J. S. Papadakis, (Springer–Verlag, New York, 1977).
14. E. A. CODDINGTON AND N. LEVINSON, Theory of Ordinary Differential Equations (McGraw–Hill, New York, 1955).
15. J. F. MILLER AND F. INGENITO, "Normal Mode FORTRAN Programs for Calculating Sound Propagation in the Ocean," NRL Memorandum Report 3071, 1975 (unpublished).
16. F. M. LABIANCA, *J. Acoust. Soc. Amer.* **53**, 1137 (1973).
17. C. T. TINDLE AND K. M. GUTHRIE, *J. Sound Vibration* **34**, 291 (1974).